A Stochastic Four-State Model of Contingent Gating of Gap Junction Channels Containing Two "Fast" Gates Sensitive to Transjunctional Voltage

Nerijus Paulauskas,[†§] Mindaugas Pranevicius,[‡] Henrikas Pranevicius,[§] and Feliksas F. Bukauskas[†*]
[†]Dominick P. Purpura Department of Neuroscience, and [‡]Anesthesiology, Albert Einstein College of Medicine, The Bronx, New York; and [§]Kaunas University of Technology, Kaunas, Lithuania

ABSTRACT Connexins, a family of membrane proteins, form gap junction (GJ) channels that provide a direct pathway for electrical and metabolic signaling between cells. We developed a stochastic four-state model describing gating properties of homotypic and heterotypic GJ channels each composed of two hemichannels (connexons). GJ channel contain two "fast" gates (one per hemichannel) oriented opposite in respect to applied transjunctional voltage (V_j). The model uses a formal scheme of peace-linear aggregate and accounts for voltage distribution inside the pore of the channel depending on the state, unitary conductances and gating properties of each hemichannel. We assume that each hemichannel can be in the open state with conductance $\gamma_{h,o}$ and in the residual state with conductance $\gamma_{h,res}$, and that both $\gamma_{h,o}$ and $\gamma_{h,res}$ rectifies. Gates can exhibit the same or different gating polarities. Gating of each hemichannel is determined by the fraction of V_j that falls across the hemichannel, and takes into account contingent gating when gating of one hemichannel depends on the state of apposed hemichannel. At the single-channel level, the model revealed the relationship between unitary conductances of hemichannels and GJ channels and how this relationship is affected by $\gamma_{h,o}$ and $\gamma_{h,res}$ rectification. Simulation of junctions containing up to several thousands of homotypic or heterotypic GJs has been used to reproduce experimentally measured macroscopic junctional current and V_j-dependent gating of GJs formed from different connexin isoforms. V_j-gating was simulated by imitating several frequently used experimental protocols: 1), consecutive V_j steps rising in amplitude, 2), slowly rising V_j ramps, and 3), series of V_j steps of high frequency. The model was used to predict V_j-gating of heterotypic GJs from characteristics of corresponding homotypic channels. The model allowed us to identify the parameters of V_j-gates under which small changes in the difference of holding potentials between cells forming heterotypic junctions effectively modulates cell-to-cell signaling from bidirectional to unidirectional. The proposed model can also be used to simulate gating properties of unapposed hemichannels.

INTRODUCTION

Connexins (Cxs), a large family of membrane proteins, form gap junction (GJ) channels that provide a direct pathway for electrical and metabolic signaling between cells. Each GJ channel is composed of two hemichannels, hexamers of Cxs also called connexons. Cell-cell communication can be organized through homotypic (same Cx isoform in both hemichannels), heterotypic (two Cx isoforms form GJ channels, but each hemichannel is assembled from one isoform) and heteromeric (different Cx isoforms form at least one hemichannel) GJ channels that vary in conductance, perm-selectivity, and gating properties. Gap junctional communication play important roles in many processes, such as impulse propagation in the heart, communication between neurons and glia, metabolic exchange between cells in the lens that lack blood system, organ formation during development, and regulation of cells proliferation (reviewed in (1–4)).

A property that appears to be common to GJ channels formed of any Cx isoform is sensitivity of junctional conductance, g_j, to transjunctional voltage, V_j (5,6). A common feature of V_j-gating is that steady-state g_j (g_{ss}) does not decline to zero with increasing V_j, but reaches a plateau or residual conductance that varies from ~5% to 30% of the maximum g_j depending on the Cx isoforms (7). Single-channel studies have shown that residual g_j is due at least in part to incomplete closure of the GJ channel by V_j, i.e., V_j causes channels to close to a subconductance (residual) state with fast gating transitions (~1 ms and less), which has significantly longer dwelling time than other substates (7,8). The symmetric reduction in g_j with positive or negative V_j has been explained by having a V_j gate in each apposed hemichannel so that for each polarity of V_j, closure can be ascribed to one or the other hemichannel (9). It was shown that V_j as well as chemical uncouplers can also induce gating transitions to the fully closed state and that these transitions are slow, ~10 ms (10,11). Gating to different levels via distinct fast and slow gating transitions led to the suggestion that there are two distinct V_j sensitive gates, termed fast and slow or ''loop'' gating mechanisms (reviewed in (12)). The fast gate closes channels to the residual state and it is mainly operated by V_j, whereas the slow gate closes channels completely and it is operated primarily by chemical uncouplers but also by V_j.

Earlier, gating properties of GJ channels were described by using Boltzmann function (9,13) assuming that GJ channels have two states, open and fully closed, as most of ionic

Submitted August 25, 2008, and accepted for publication January 14, 2009.

Nerijus Paulauskas and Mindaugas Pranevicius contributed equally to this work.

*Correspondence: fbukausk@aecom.yu.edu

Editor: Benoit Roux.

0006-3495/09/05/3936/13 $2.00

doi: 10.1016/j.bpj.2009.01.059

channels. To find gating parameters, g_j-V_j dependence was split into two segments for positive and negative V_js. Such approach allowed to describe gating properties of homotypic and heterotypic GJ channels assuming that each hemichannel gates independently, which may be accurate only when both hemichannels have the same gating polarity, have similar single-channel conductance, and are relatively insensitive to V_j. Previously there were few attempts to describe V_j gating of GJs at the single-channel level (14) and macroscopically (15) by using a four-state model in which each hemichannel contained a fast gate operating between open and residual states. Both models made a progress introducing a more detailed description of GJ channels based on most recent experimental data and improved the fitting process allowing to find gating parameters of GJ channels. However, the analytical approach used in (15) to describe V_j-gating allowed only steady-state predictions. Neither of the previous models allowed the possibility to study kinetics of junctional current during applied transjunctional voltages. Ramanan et al. (16) proposed a three-state model of Cx37 GJ channels that exhibits the main state and two substates. This model was adapted more specifically to GJ channels that demonstrate multiple substates.

Here we present a stochastic four-state model that uses imitative approach and accounts for voltage distribution inside the pore of the GJ channel, i.e., takes into account contingent gating. Each hemichannel contains a fast gating mechanism with variable gating polarity. Each gate can be in open or closed states that correspond to the open state or the residual state, respectively, of the hemichannel. In addition, unitary conductances of open and residual states depend on V_j, i.e., conductance of hemichannels rectifies. The model was used to imitate experimental data of V_j-gating in homotypic and heterotypic junctions measured in HeLa cells exogenously expressing different Cx isoforms. Our model allowed simulation of the dynamics of junctional current that was achieved due to use of stochastic description of voltage gating processes. This enhanced flexibility of the model in respect to its structure and variation of parameters used to describe the conductance and gating of hemichannels composing GJ channel.

MATERIAL AND METHODS

Cells and culture conditions

Experiments were performed using HeLa cells (Human cervix carcinoma cells, ATCC CCL2) stably transfected with different Cx isoforms (Cx31, Cx40, Cx43, Cx45, and Cx47). More details about used DNAs for transfection and selection of clones stably expressing different Cx isoforms are in (17–19). Cells were grown in Dulbecco's modified Eagle's medium supplemented with 8% fetal calf serum (Gibco, Carlsbad, CA), 100 μg/ml streptomycin and 100 units/ml penicillin.

Electrophysiological measurements

Experiments were performed in modified Krebs-Ringer solution containing (in mM): NaCl, 140; KCl, 4; $CaCl_2$, 2; $MgCl_2$, 1; glucose, 5; pyruvate, 2; HEPES, 5 (pH 7.4). Electrodes were filled with pipette solution containing (in mM): KCl, 130; NaAsp, 10; MgATP, 3; $MgCl_2$, 1; $CaCl_2$, 0.2; EGTA, 2; HEPES, 5 (pH = 7.2). For electrophysiological recordings, cells were grown onto glass coverslips and transferred to an experimental chamber mounted on the stage of an inverted microscope IX70 (Olympus, Center Valley, PA). Cells were perfused with modified Krebs-Ringer solution at room temperature. Junctional conductance (g_j) was measured in selected cell pairs using the dual whole-cell patch clamp system (20). Briefly, each cell within a pair was voltage clamped independently with a separate patch clamp amplifier (EPC-7plus; HEKA). Transjunctional voltage (V_j) was induced by stepping the voltage in cell-1 (ΔV_1) and keeping the other constant, $V_j = \Delta V_1$. Junctional current (I_j) was measured as the change in current in the unstepped cell-2, $I_j = \Delta I_2$. Thus, g_j was obtained from the ratio, $-I_j/V_j$, where negative sign indicates that junctional current measured in cell-2 is oppositely oriented to the one measured in cell-1. Signals were acquired and analyzed using custom-made software (21) and A/D converter from National Instruments (Austin, TX).

RESULTS

Initially, we will highlight the experimental data demonstrating basic properties of GJs that we used in the model. This includes micro- and macroscopic V_j-gating events, single GJ channel gating transitions between open and residual states, and their rectification. Subsequently, we will describe the model and simulate V_j-gating in homo- and heterotypic junctions composed of different numbers of GJ channels. Finally, we will simulate signal transfer asymmetry in response to electrical activity of high frequency applied to either side of heterotypic junctions.

Conductance and voltage gating properties of GJ channels formed from different Cx isoforms

Typically, homotypic GJ channels exhibit g_j decay in response to V_j and symmetric g_{ss}-V_j dependence. Fig. 1 *A* shows I_j through Cx47 homotypic channels evoked by negative V_j steps of 31, 48, and 65 mV. Short and repeated voltage steps of $\pm$18 mV (see the inset) were used to measure g_j in between of long V_j steps. During V_j steps of $-$48 and $-$65 mV, I_j decayed from an initial value (I_{in}) to a steady-state level (I_{ss}). Fig. 1 *B* shows averaged and normalized G_{in} and G_{ss} (normalized to g_j at V_j = 0 mV) dependencies on V_j. G_{in}-V_j plot (*solid circles*; *dashed line* is a regression line of the second order) shows virtually no changes of G_{in} over V_j range from $-$110 to 110 mV. G_{ss}-V_j plot demonstrates symmetric bell-shape dependence on V_j that is typical for homotypic GJ channels. The solid line is a fit of G_{ss} data to Boltzmann's equation (13). The fit was performed separately for g_{ss} data at positive and negative V_js. Fig. 1 *C* shows variation of G_{ss}-V_j dependence among different Cx isoforms forming homotypic GJ channels.

Fig. 2 shows I_j record of HeLaCx47 cell pair exhibiting one functional channel. Solid gray lines show that during first two ramps, the channel is open and I_j is virtually linear over applied V_js. At the beginning of the third ramp, channel closes from the open state to the substate or the residual state and remains closed during period indicated in the box. The inset shows that I_j-V_j relationship is not linear and rectifies

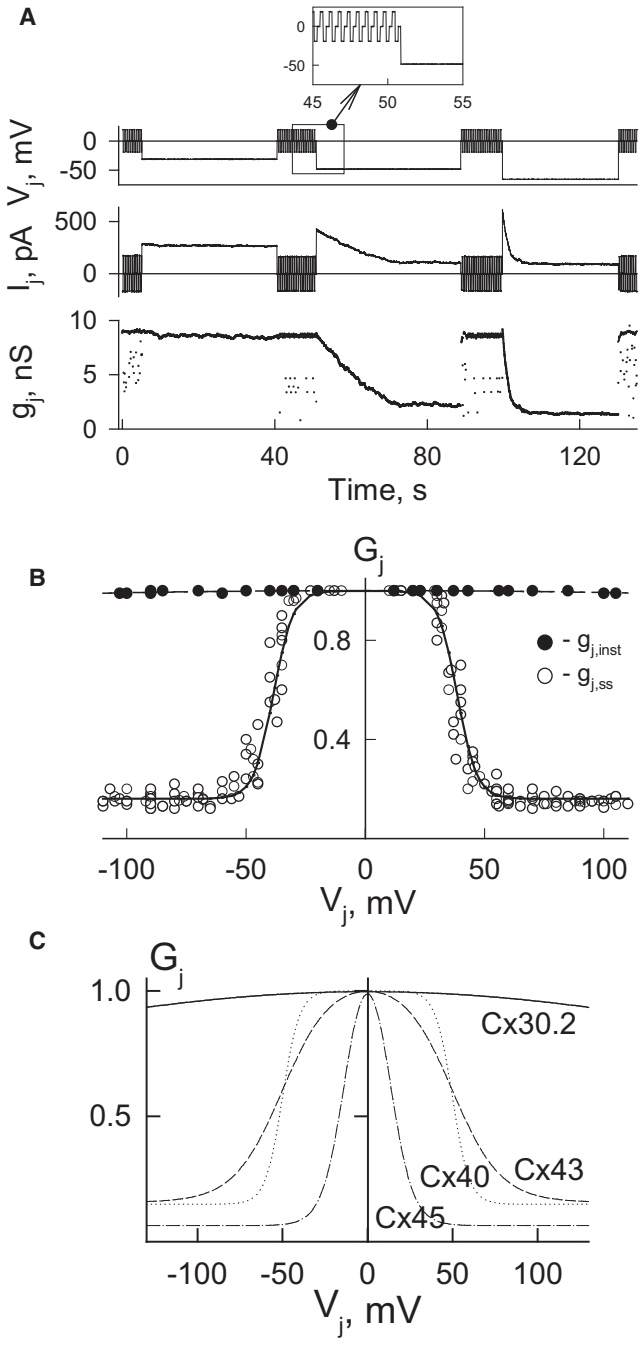

FIGURE 1 Illustration of voltage gating in HeLa cells expressing different Cx isoforms. (*A*) An example of I_j decay in homotypic Cx47 channels evoked by negative V_j steps of 31, 48, and 65 mV. Repeated voltage steps of ±18 mV (see the *inset*) were used to measure g_j in between of long V_j steps. (*B*) Dependencies of G_{in} and G_{ss} (normalized to g_j at $V_j = 0$ mV) on V_j in Cx47 homotypic GJs. (*C*) G_{ss}-V_j plots of different Cx isoforms forming homotypic GJ channels.

almost exponentially. The rectification of the residual state was shown earlier for Cx43 (22) and Cx32 (23) GJ channels. The rectification of the open state is problematic to monitor in homotypic GJ channels because conductances of apposed hemichannels are oriented as mirror images of each other.

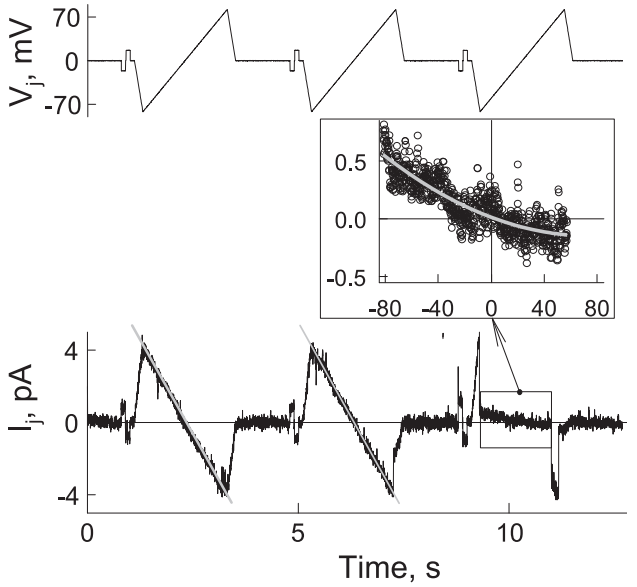

FIGURE 2 Illustration of the rectification of the residual conductance in HeLaCx47 cell pair exhibiting one functional channel. Solid gray lines on I_j trace show that during first two ramps the channel is open, and I_j is virtually linear over entire V_j range. During the third ramp, the channel was closed to the residual state over time indicated in the box. The inset shows that I_j-V_j relationship of the residual state is not linear, i.e., rectifies.

Otherwise, $g_{h,o}$ rectification was well documented in unapposed hemichannels of Cx30, Cx46, and Cx50 (24,25).

Heterotypic GJ channels that form between cells expressing different connexins (each cell expresses one Cx isoform) typically exhibits asymmetric V_j-gating. Fig. 3 *A* shows currents through Cx43/Cx45 heterotypic GJ channels at V_j ramps from +60 to −60 mV applied to HeLaCx43 cell. At positive V_js the channel exhibits gating transitions between open and closed states, whereas at negative V_js the channel stays open. Summarized I_j-V_j plot shows that I_j of the open state is virtually linear over V_j, that the channel exhibits strong V_j-gating asymmetry and that gating transitions were observed preferentially at V_js negative on Cx45 side. This is in agreement with our previous report demonstrating that the gating polarity of Cx45 is negative (26). However, not all heterotypic junctions show linear I_j-V_j relationship for the open state. Fig. 3 *B* shows I_j record of the single Cx32/Cx46 heterotypic channel in response to repeated series of V_j steps and ramps. Summarized I_j-V_j plot shows that the open state demonstrates very strong rectification (the *solid gray line* is a fit of the data points representing the open state to the exponential function); I_j at $V_j = +90$ mV is ~3-fold smaller than at $V_j = -90$ mV.

Fig. 4 shows V_j-gating of Cx31/Cx45 heterotypic junction examined by using voltage ramps with slow rise of V_j over time. The I_j trace shows strong asymmetry, similar to that reported earlier (27), in response to two V_j ramps of different polarity. Earlier, we reported that in some heterotypic GJs an asymmetry of g_j-V_j plots is higher than predicted from intrinsic V_j-gating sensitivities of Cxs composing heterotypic

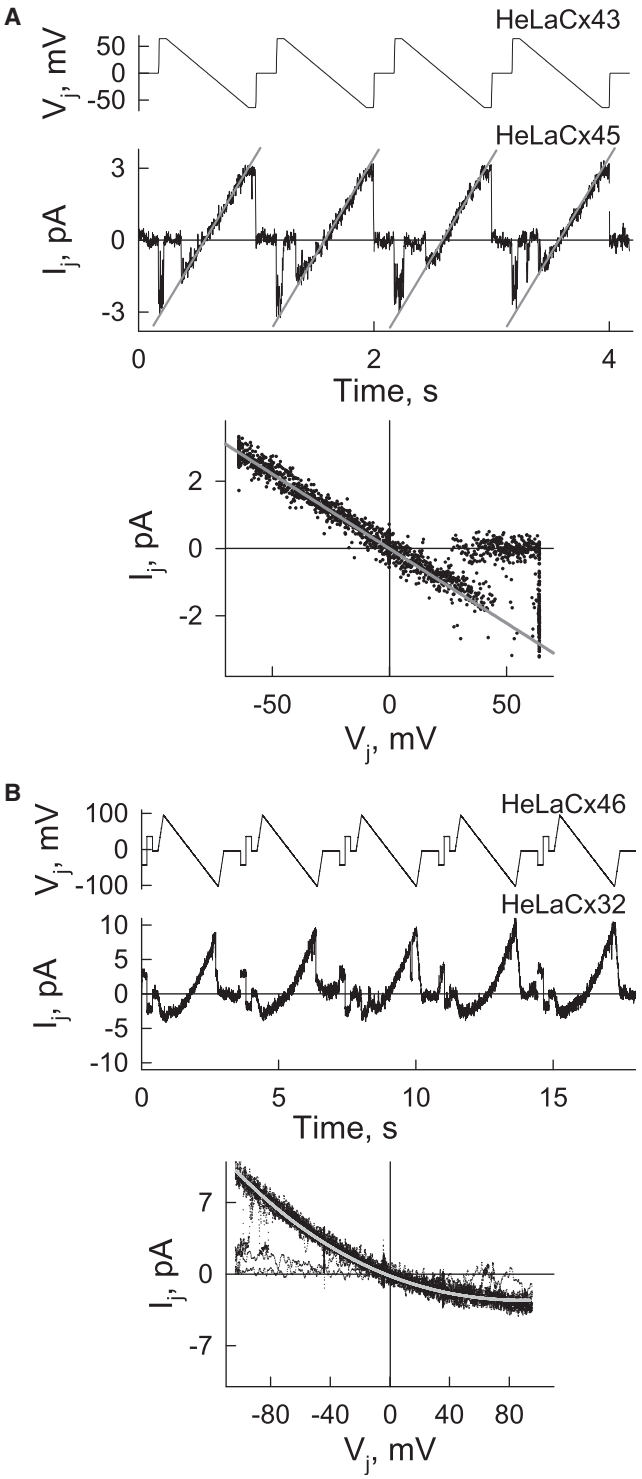

FIGURE 3 I_j recordings at the single-channel level demonstrating an absence and presence of I_j-V_j rectification of the open state in Cx43/Cx45 (*A*) and Cx32/Cx46 (*B*) heterotypic junctions, respectively.

GJ channels (26,27). We hypothesized that a difference in unitary conductances of hemichannels affects asymmetry of g_j-V_j plot. We will exploit the model by using voltage ramp protocol to study V_j-gating to validate this statement (see Fig. 10).

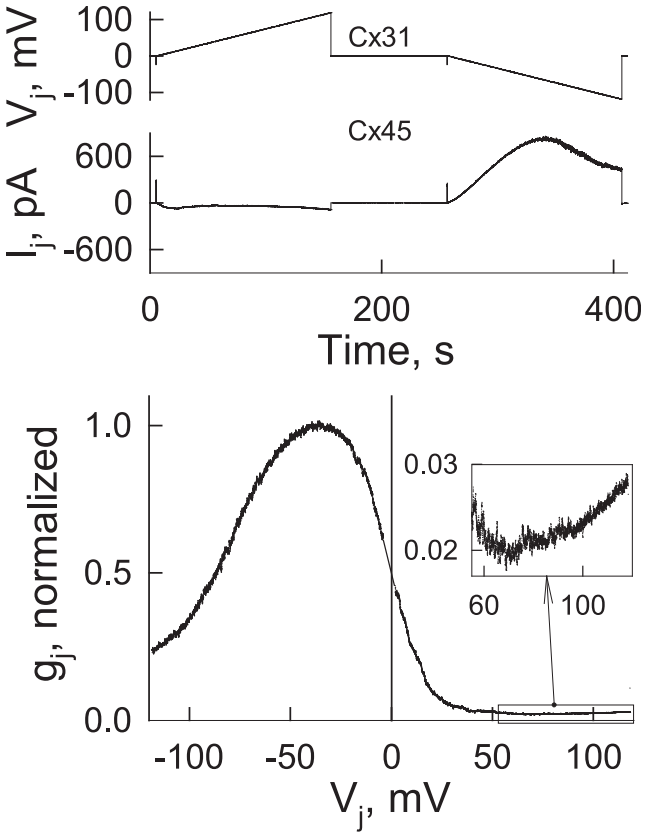

FIGURE 4 V_j-gating in HeLa cell pair forming Cx31-EGFP/Cx45 heterotypic junctions. I_j trace shows strong asymmetry of I_j response to V_j ramps slowly rising from 0 to −115 mV and from 0 to 115 mV. G_j-V_j plot (normalized to maximal g_j at $V_j = \sim -40$ mV) shows that at $V_j = 0$ only ~50% of Cx31-EGFP/Cx45 channels are open. Data shown in the inset demonstrate an increase of g_j at V_js >60 mV.

The g_{ss}-V_j plot calculated from V_j and I_j traces allows us to suggest that at $V_j = 0$ only a fraction (<1/2) of Cx31/Cx45 channels are open and g_{ss} increases when the Cx45 side is relatively more positive and decreases almost to zero when the Cx45 side is more negative. Similar g_j-V_j gating asymmetry was documented in other heterotypic junctions, such as Cx43/Cx45 (26) and Cx40/Cx45 (20). Interestingly, the data shown in the inset demonstrate that when V_j increased from 60 to 110 mV, g_{ss} increased. This phenomenon was reproduced in the model by assuming a presence of conductance rectification of the residual state of Cx45 (see Fig. 9 *E*).

In summary, heterotypic GJs in contrast to homotypic GJs demonstrate asymmetric V_j-gating. V_j-gating of GJ channel depends on intrinsic gating properties of composing hemichannels as well as on the fraction of V_j that drops on each of them. This fraction is 1/2 for open homotypic GJ channels, and it can be very different for heterotypic GJ channels formed from Cxs that demonstrate different unitary conductances. In addition, data shown in Figs. 2 *B* and 3 *B* demonstrate that I_j-V_j relationship of the single channel of open and residual states can rectify. Thus, in the model, we should take

into account Cx-type dependent V_j-gating sensitivity, unitary conductances of open and residual states, as well as their I/V rectification.

Description of the model

Schematics of transitions between states

In the model, we assume that the GJ channel is formed from *A* and *B* hemichannels, and each hemichannel contributes one voltage-sensitive gate that closes channels to the residual state, i.e., imitates the fast gating mechanism (12). Therefore, in concert with previous models (13–15), we assume that two voltage gates in series control the gating of GJ channel (Fig. 5 *A*). The schematic presentation of the four-state model is shown in Fig. 5 *B*, where K_i ($i = 1, 2, 3, 4$) are equilibrium constants for each of transitions between states. The channel can occupy one of the four possible states: 1), AoBo, both gates are open, 2), AcBo, *A* gate is closed and gate *B* is open, 3), AoBc, *A* gate is open and *B* gate is closed, and 4), AcBc, both gates are closed.

The equilibrium constants between the states were described as exponential functions that depend on transjunctional voltage across the hemichannels *A* and *B* (V_A and V_B; we assume that transjunctional voltage across the gate and hemichannel is the same):

$$\begin{aligned} K_1 &= e^{A_1(-\Pi \cdot V_A - V_{01})} \\ K_2 &= e^{A_2(\Pi \cdot V_B - V_{02})} \\ K_3 &= e^{A_3(-\Pi \cdot V_A - V_{03})}, \\ K_4 &= e^{A_4(\Pi \cdot V_B - V_{04})} \end{aligned} \quad (1)$$

where A_i is the voltage sensitivity coefficient; V_{oi} is the voltage for half-maximal conductance; and Π is a gating polarity, which can be positive or negative. Negative and positive signs for V_A and V_B, respectively, indicate that the two gates are oriented as mirror images of each other. Transjunctional voltage across the GJ channel is a sum of V_A and V_B, i.e., $V_j = V_A + V_B$. Closing one hemichannel changes the voltage across the apposing hemichannel, and this will affect the probability of changing the state. Thus, the model exploits principles of contingent gating. Aggregate method was used for a formal description of the model and consequently for writing the algorithm (see Supplement 2 in the Supporting Material). The piece-linear aggregate is described in accordance with Markov principles, i.e., the probability of transitions does not depend on the history of previous transitions. The algorithm was written using C Sharp ($C^{\#}$) programming language.

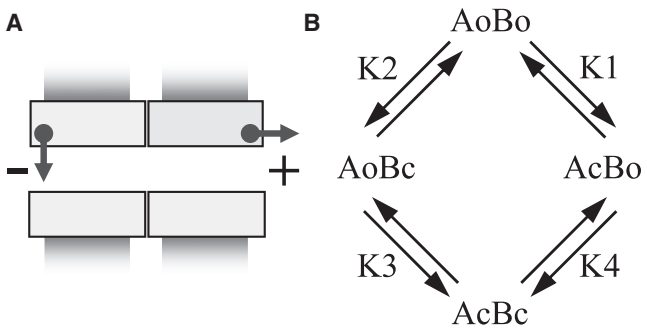

FIGURE 5 Schematics of the four-state model. (*A*) The scheme of the GJ channel containing the fast gate in each hemichannel. (*B*) Illustration of a four-state model: 1), AoBo—both gates are open, 2), AcBo—gate A closed and gate B open, 3), AoBc—gate A open and gate B closed, and 4), AcBc—both gates closed. K_i ($I = 1$–4) are equilibrium constants.

Assuming that both gates do not interact with each other except via voltage redistribution inside the pore and only voltage across each of *A* and *B* hemichannels defines their gating, then $A_1 = A_3$, $A_2 = A_4$, $V_{01} = V_{03}$, and $V_{02} = V_{04}$. As reported earlier (15), regardless of the pathway of transitions between states AoBo and AcBc, thermodynamic law requires that $K_1 \times K_4 = K_2 \times K_3$. Following the scheme shown in Fig. 5 *B*, opening and closing probabilities of gate *A* depend on K_1: $P(A_{o\to c}) = K_1 \times P(A_{c\to o})$. We will define such a small time interval, Δt, at which only one transition for each gate is possible. Interval Δt will be used as a simulation step. For example, when $K_1 = 1$, both open and closed states of the gate are equally possible, $P(A_o) = P(A_c)$. When system is at equilibrium, average number of open and closed gates does not change. Thus, the average number of opening and closing events of the gate must be equal or $P(A_o) \times P(A_{o\to c}) = P(A_c) \times P(A_{c\to o})$. If we label $P\kappa$ as a probability that the gate will change the state during time interval Δt, then $P\kappa = P(A_o) \times P(A_{o\to c}) + P(A_c) \times P(A_{c\to o})$. When both states are equally probable ($K_1 = 1$), then $P(A_o) = P(A_c) = 1/2$ and $P\kappa = (P(A_{o\to c}) + P(A_{c\to o}))/2$. The difference, $1 - P\kappa$, is a probability that the gate will stay in the same state. In general, the model defines at any given time whether individual channels remain in the same state or change the state. In junction composed of thousands of GJ channels any new calculation at the same V_j protocol results to random distribution of open and closed states over time for individual channels while the mean g_j remains the same.

Conductance of hemichannels

The proposed model assumes that each hemichannel can be in the open or the closed states with conductances, $\gamma_{h,o}$ and $\gamma_{h,res}$, respectively. Studies of the single GJ channel formed of various Cx isoforms show that the ratio of γ_{res}/γ_o is in the range of 0.2–0.25. The ratio, $\gamma_{h,res}/\gamma_{h,o}$, for hemichannels should be different and for homotypic GJs $\gamma_{res}/\gamma_o = 2(\gamma_{h,res}/\gamma_{h,o})/(1+\gamma_{h,res}/\gamma_{h,o})$. However, this relationship could be more complex if both $\gamma_{h,o}$ and $\gamma_{h,res}$ depend on V_j, i.e., when they demonstrate rectifying properties as it is shown in Figs. 2 *B* and 3 *B*. Similar to (14), we used single exponential function to describe $\gamma_{h,o}$ and $\gamma_{h,res}$ dependence on V_j: $\gamma_{h,o} = \Gamma_o e^{(-V_j/\varpi_o)}$ and $\gamma_{h,res} = \Gamma_{res} e^{(-V_j/\varpi_{res})}$, where Γ_o and Γ_{res} are unitary conductances of hemichannels at $V_j = 0$ mV, and ϖ_o and ϖ_{res} determine rectification constant.

We generated three versions of the model that differ in stimulation protocols: 1), consecutive V_j steps rising in the

amplitude, 2), slowly raising V_j ramps, and 3), series of short negative and positive V_j steps of variable frequency. In Supplement 1 in the Supporting Material, we show examples of the screen captures for each of used protocols (see Fig. S1, Fig. S2, and Fig. S3).

Simulation of homotypic GJ channels

Single-channel gating

Fig. 6 *A* shows I_j recordings in response to three consecutive V_j steps of −20, −60, and −100 mV. We assumed that the cell pair forms single homotypic GJ channel with parameters identical for both hemichannels: $V_{h,o} = 40$ mV $\gamma_{h,o} = 200$ pS, $\gamma_{h,res} = 25$ pS, $A_h = 0.05$ mV^{-1} ($V_{h,o}$ corresponds to V_{oi}, and A_h corresponds to A_A or A_B in Eq. 1; in homotypic GJ channel $A_A = A_B$ and $V_{o,A} = V_{o,B}$). In addition, it was assumed that both open and residual states do not rectify, i.e., $\varpi_o = \infty$ and $\varpi_{res} = \infty$. I_j traces show that open channel probability decays with V_j increase, and three conductance states can be distinguished, which are best seen in I_j trace at $V_j = 100$ mV. When the channel is fully open, $I_j = 10$ pA. When one hemichannel is closed to the residual state ($I_j = 2.2$ pA), we call this state as a primary residual state. The arrow shows the substate that we call the secondary residual state when two gates are closed ($I_j = 1.3$ pA). An overlay of g_j traces for all three voltage steps show that γ_o=100 pS, whereas γ_{res} is equal 22 pS for the primary residual state and 13 pS for the secondary residual state. When the ratio $\gamma_{h,res}/\gamma_{h,o} = 0.125$ (25 pS/200 pS) then for the primary residual state $\gamma_{res}/\gamma_o = 0.222$ (22.2 pS/100 pS). Experimental data show that for different connexins γ_{res}/γ_o is in between 0.2 and 0.25 (12). According to the model, to cover this range of γ_{res}/γ_o, the ratio, $\gamma_{h,res}/\gamma_{h,o}$, should be in the range of 0.111–0.143, i.e., ~2-fold smaller.

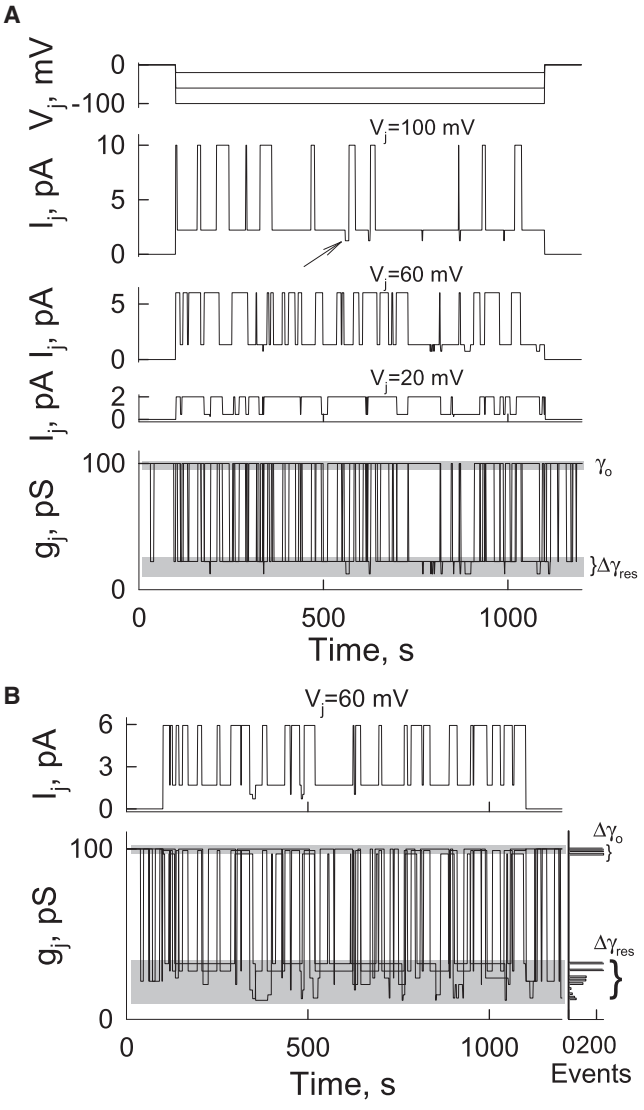

FIGURE 6 Simulation of the junction containing single homotypic GJ channel. The following parameters were identical for both hemichannels: $V_{h,o} = 40$ mV, $\gamma_{h,o} = 200$ pS, $\gamma_{h,res} = 25$ pS, and $A_h = 0.05$ mV^{-1}. (*A*) I_j and g_j traces of nonrectifying channel simulated at three V_j steps of −20, −60, and −100 mV. g_j trace is an overlay of conductances calculated for all three voltage steps. (*B*) I_j and g_j traces of the channel exhibiting $\gamma_{h,o}$ and $\gamma_{h,res}$ rectification with ϖ_o= 400 mV and $\varpi_{res} = 200$ mV. I_j trace shows single channels gating at $V_j = -60$ mV. The bottom g_j trace shows overlay of conductances at V_j steps of −20, −60, and −100 mV.

Fig. 6 *B* shows an example of I_j trace of the single channel at $V_j = 60$ mV. All parameters are the same as in Fig. 6 *A* but the open and residual states exhibit I/V rectification with ϖ_o = 400 mV and $\varpi_{res} = 200$ mV. g_j trace obtained superposing g_js at three V_js, as in Fig. 6 *A*, demonstrates that both γ_o is γ_{res} are not constant. Next to g_j trace, we show the frequency histogram, which demonstrates that at these particular V_js three states can be distinguished for γ_o and nine states for γ_{res}. Repeated simulations, which results in stochastic data sets, show that we are getting 96, 98, and 99 pS for γ_o and more substate conductances in the range of 9–25 pS. Therefore, I/V rectification can result to a large variety of γ_o and γ_{res} measured experimentally at different V_js.

In summary, for homotypic nonrectifying GJ channel, we can expect having one conductance for γ_o and two conductances for γ_{res}. The ratio, $\gamma_{h,o}/\gamma_{h,res}$, for hemichannels is approximately twice smaller than ratio, γ_o/γ_{res}, for GJ channel. If hemichannels exhibit I/V rectification of open and residual states, then in GJ channel both γ_o and γ_{res} depend on applied V_js, but γ_{res} varies in broader range than γ_o.

V_j-gating of homotypic junctions

Fig. 7 shows theoretically predicted G_j (normalized to g_j at $V_j = 0$) dependences on V_j. In these calculations, we used identical set of parameters for both hemichannels ($\gamma_{h,o} = 200$ pS, $\gamma_{h,res} = 25$ pS, $V_{h,o} = 40$ mV $A_h = 0.1$ mV^{-1}, $\varpi_o = \infty$ and $\varpi_{res} = \infty$) and for each plot only one parameter of six varied. For a clearer description, the hemichannels forming GJ channels were attributed to the left- and right-side hemichannels. In all plots, the same color represents different measured parameters: 1), black lines for G_{in}; 2), gray lines for G_{ss}; 3), blue and red lines for the right-side and the left-side hemichannels,

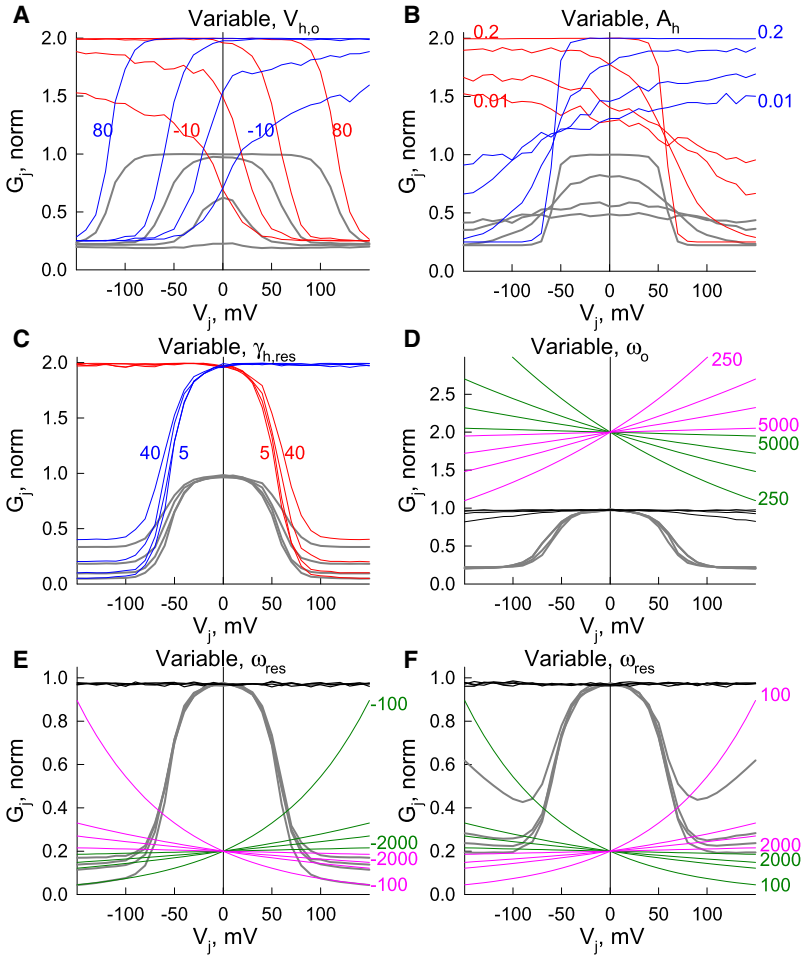

FIGURE 7 Simulated g_j-V_j dependencies of homotypic junctions containing 1000 GJ channels; data were normalized to g_j values at $V_j = 0$ mV. Identical set of parameters were used for both hemichannels ($\gamma_{h,o} = 200$ pS, $\gamma_{h,res} = 25$ pS, $V_{h,o} = 40$ mV, A_h=0.1 mV^{-1}, $\varpi_o = \infty$, and $\varpi_{res} = \infty$) and in each plot only one parameter of six varied. Measured parameters are shown in different colors: 1), black for G_{in}; 2), gray for G_{ss}; 3), blue and red for g_j of the right-side and the left-side hemichannels, respectively; and 4), pink and green for $\gamma_{h,o}$ and $\gamma_{h,res}$ rectification of the left-side and the right-side hemichannels, respectively. (*A*) G_{ss}-V_j plots at $V_{h,o}$ of 80, 40, 10, and −10 mV. (*B*) G_{ss}-V_j plots at A_h of 0.2, 0.05, 0.02, and 0.01 mV^{-1}. (*C*) G_{ss}-V_j plots at $\gamma_{h,res}$ of 40, 20, 10, and 5 pS. (*D*) G_{in}-V_j and G_{ss}-V_j plots at different extent of $\gamma_{h,o}$ rectification, $\varpi_{h,o}$ = 5000, 1000, 500, or 250 mV. (*E*, *F*) G_{in}-V_j and G_{ss}-V_j plots at different extent of $\gamma_{h,res}$ rectification, $\varpi_{h,res}$=2000, 500, 300, or 100 mV.

respectively; and 4), pink and green lines for $\gamma_{h,o}$ and $\gamma_{h,res}$ rectification of the left-side and the right-side hemichannels, respectively. In all calculations the number of GJ channels (N) was equal to 1000.

Fig. 7 *A* demonstrates that when $V_{h,o}$ of left- and right-side hemichannels changed from 80 to 40 mV, there was mainly reduction in the width of G_{ss}-V_j plot but little in g_{max}. Further reduction of $V_{h,o}$ to 10 and −10 mV led to the strong reduction of g_{max}. At $W_{ho} = -10$ mV GJs almost lost V_j dependence with g_j being close to g_{min}. Supplement 1, Fig. S4, in the Supporting Material demonstrates how G_j-V_j plots shown in Fig. 7 *A* were acquired.

Fig. 7 *B* demonstrates that the reduction of A_h from 0.2 to 0.05, 0.02, and 0.01 mV^{-1} strongly affected the steepness of G_{ss} decline ($\Delta G_{ss}/\Delta V_j$) around $V_j = 40$ and −40 mV and reduced g_{max}. At $A_h = 0.01$ mV^{-1}, G_{ss} shows very weak dependence on V_j.

Fig. 7 *C* demonstrates that reduction of $\gamma_{h,res}$ from 40 to 20, 10 and 5 pS substantially affected g_{min} but not g_{max}. We did not show simulations with changes of $\gamma_{h,o}$, which always was equal 200 pS, because the character of g_j-V_j plots mainly depends on the ratio, $\gamma_{h,o}/\gamma_{h,res}$, rather than on the absolute values of $\gamma_{h,o}$ and $\gamma_{h,res}$.

Fig. 7 *D* demonstrates that $\gamma_{h,o}$ rectification at $\varpi_{h,o}$s between 500 and 5000 mV did not visibly affect G_{in}-V_j dependence until $\varpi_{h,o} < 300$ mV. Therefore, even though $\gamma_{h,o}$ rectifies substantially, it is difficult to detect its effect on G_{in}-V_j plot until this rectification is very significant that may not be physiological. G_{in}-V_j dependence remains the same independent on the direction of $\gamma_{h,o}$ rectification, i.e., whether $\gamma_{h,o} = e^{(-V_j/\varpi_o)}$ or $\gamma_{h,o} = e^{(V_j/\varpi_o)}$. Fig. 7 *D* shows that $\varpi_{h,o}$ has a relatively small effect of G_{ss}-V_j plot.

Fig. 7, *E–F*, demonstrate that $\gamma_{h,res}$ rectification had no evident effect on G_{in} but affected most significantly G_{ss} at V_js exceeding ±80 mV, i.e., g_{min}. Rectification of $\gamma_{h,res}$ was changed by attributing to ϖ_{res} values from 2000 to 100 mV (see *pink and green lines*). In both plots, $\gamma_{h,res}$ rectifies but in plot *E* $\gamma_{h,res} = e^{(-V_j/\varpi_{res})}$ and in plot *F* $\gamma_{h,res} = e^{(V_j/\varpi_{res})}$, i.e., $\gamma_{h,res}$ decreased or increased, respectively, with increase of V_j. Plots *E* and *F* show that g_{min} tends to continuously decay and increase, respectively, at higher V_js.

Fig. 8 shows I_j trace that was obtained from simulation of V_j-gating in response to long V_j ramps from 0 to 150 mV and from 0 to −150 mV. We examined how the steepness of V_j ramps affects g_{ss}. We did this experiment by holding the same amplitude of voltage ramps but shortening their

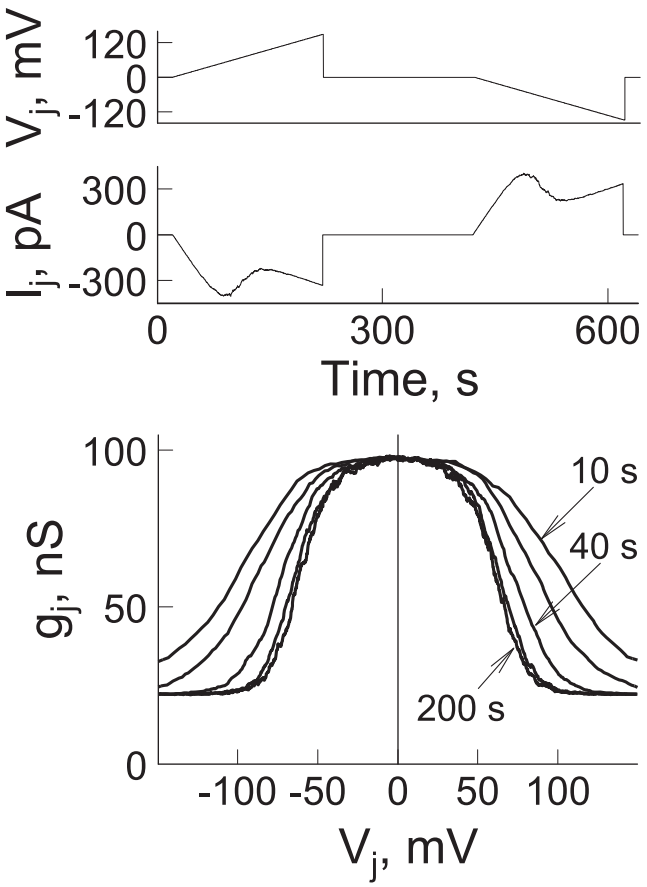

FIGURE 8 Simulation of V_j-gating in homotypic GJs in response to slowly rising V_j ramps from 0 to +150 and from 0 to −150 mV. The slope of ramps was changed by shortening their duration from 200 to 100, 40, 20, and 10 s.

duration stepwise from 200 to 100, 40, 20, and 10 s. At durations of V_j ramps longer than 200 s, g_{ss}-V_j plots practically overlapped (not shown) and were identical to that measured by applying consecutive V_j steps of ~30 s or longer. When V_j steps are used, it is possible to visualize whether steps are long enough (T_{min}) to reach the steady state that is not so obvious with the use of V_j ramps. At V_j ramps shorter than 100 s, g_{ss}-V_j plots become broader suggesting that steady state of g_j was not yet reached. Our data show that to reach the steady state, the duration of V_j ramps should be several times longer than T_{min} used for V_j steps. In experimental studies, it is preferable to use slowly raising voltage ramps instead of consecutive V_j steps because it requires less time to measure g_{ss}-V_j plot and it is continuous over entire V_j range. Thus, the model can be used to predict an optimal length of V_j ramps for V_j-gating studies in cells expressing different Cx isoforms.

In summary, data shown in Figs. 7 and 8 demonstrate the influence that each of the independent parameters has on the gating properties of homotypic GJ channels. Shown data demonstrate a consistency independently whether consecutive V_j steps or slow V_j ramps were used to study V_j-gating properties of GJ channels.

V_j-gating of heterotypic junctions

Fig. 9 shows the g_j-V_j plot of a heterotypic junction. In this simulation, we used two sets of parameters (see Fig. 9 *A*) that are close to those of Cx43 (cell-1) and Cx45 (cell-2). Of all heterotypic junctions, the V_j-gating properties of Cx43/Cx45 junctions are among the most examined (28,26). Fig. 9 *B* shows the protocol used to simulate g_j-V_j dependence. I_j was calculated in response to consecutive V_j steps increasing stepwise ($\Delta V_j = 20$ mV) from −100 to 100 mV. g_j trace shows that during time period from 0 to 30 s ($V_j = 0$ mV) g_j decayed from ~50 nS reaching the steady state at 39 nS. This decay is caused by the fact that at the starting point we always assumed that GJ channels are fully open and time window of ~10–30 s was used to allow the system to reach the steady state before V_j protocol was applied. g_{ss}-V_j plot (Fig. 9 *C*; *gray line*) calculated with the parameters shown in panel *A* demonstrates a strong V_j-gating asymmetry. The family of g_{ss}-V_j plots show that an asymmetry of V_j-gating increased with the reduction of $V_{h,o}$ of Cx45 from 30 to 10, −10, −30, and −50 mV. We observed similar changes in Cx43/Cx45 GJs during acidification of the cytoplasm (F. F. Bukauskas, unpublished data).

To assess an effect of conductance rectification on V_j-gating, we varied ϖ_o and ϖ_{res}, whereas other parameters remained the same as shown in Fig. 9 *A*. Fig. 9 *D* demonstrates that reduction of ϖ_o from 5000 (*circles*) to 500 (*diamonds*) and 250 mV (*triangles*) has small effect on g_{ss}-V_j dependence (*gray lines*) but increased steepness of g_{in}-V_j plots (*black lines*). Interestingly, similar changes of ϖ_o did not affect substantially g_{in} of homotypic junctions (see Fig. 7 *D*). Therefore, an effect of $\gamma_{h,o}$ rectification on g_{in} is obscured in homotypic junctions and is more expressed in heterotypic junctions. Fig. 9 *E* demonstrate that reduction of ϖ_{res} from 4000 (*circles*) to 400 (*diamonds*) and 200 mV (*triangles*) did not affect g_{in}-V_j dependence (*black lines*) but modified g_{ss}-V_j plots (*gray lines*) at higher V_js. The inset in Fig. 9 *E* highlights g_{ss} increase with increase of V_j. We observed similar phenomena in Cx45/Cx31 (27), Cx45/Cx40 (20), and Cx45/Cx43 (26) junctions (see also the inset in Fig. 4). Therefore, the model allows us to suggest that this g_{ss} increase may be caused, at least in part, by $\gamma_{h,res}$ rectification.

Previously, V_j-gating asymmetry was commonly used to determine the gating polarity of Cxs composing heterotypic junctions (29,30). This practice was based on an assumption that V_j-gating of heterotypic junctions at different V_j polarities reflects intrinsic gating properties of composing hemichannels. We tested this by superposing simulated g_{ss}-V_j plot of heterotypic junction with those corresponding to homotypic junctions. Gray lines in Fig. 10 *A* show g_{ss}-V_j plots of Cx43 and Cx45 homotypic junctions with parameters shown in Fig. 9 *A*. Solid black line 1 shows g_{ss}-V_j plot of heterotypic junction with parameters used for simulation of corresponding homotypic junctions. To examine how the difference in unitary conductances of composing hemichannels affect

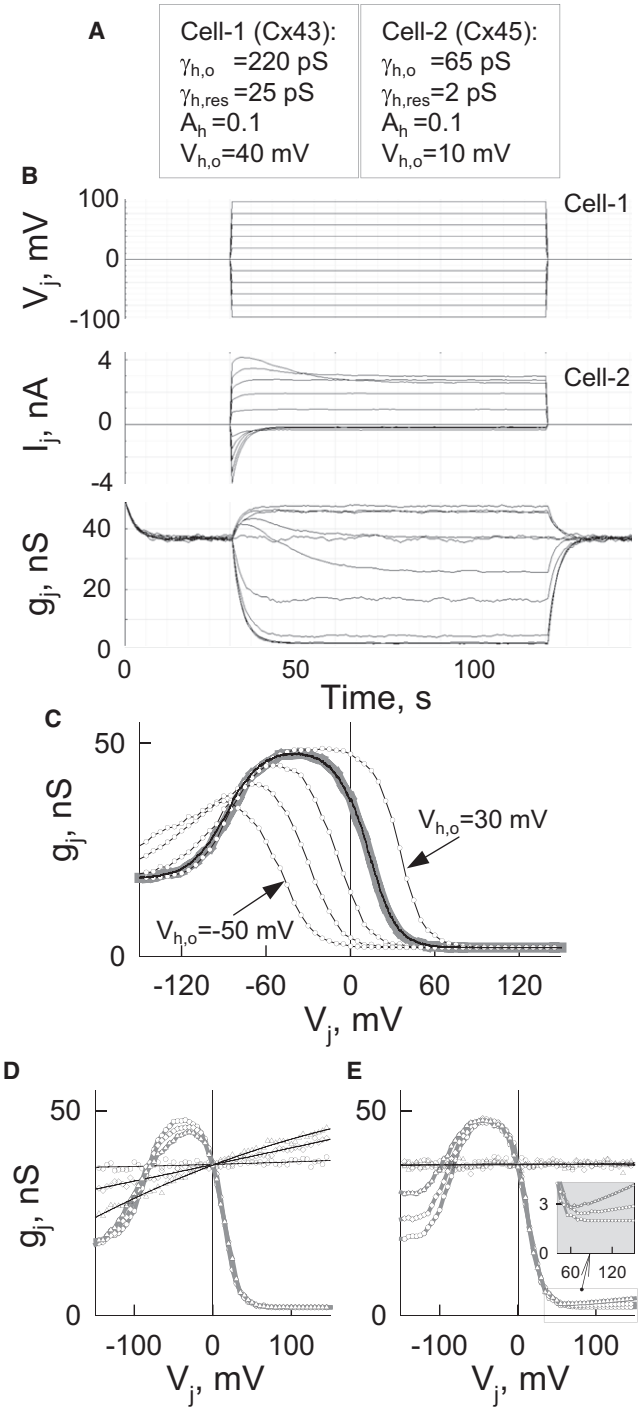

FIGURE 9 G_j-V_j plots of heterotypic junction. Two sets of parameters shown in *A* were used for this simulation. (*B*) I_j and g_j traces were calculated in response to consecutive V_j steps increasing stepwise ($\Delta V_j = 20$ mV) from −100 to 100 mV. (*C*) The family of g_{ss}-V_j plots show that V_j-gating asymmetry increased with the reduction of $V_{h,o}$ of Cx45 from 30 to 10 (*thick gray line*), −10, −30, and −50 mV. (*D* and *E*) An effect of $\gamma_{h,o}$ and $\gamma_{h,res}$ rectification on V_j-gating. g_{ss}-V_j (*gray lines*) and g_{in}-V_j (*black lines*) plots shown in *D* were obtained at ϖ_o of 5000 (*circles*), 500 (*diamonds*), and 250 mV (*triangles*). g_{ss}-V_j (*gray lines*) and g_{in}-V_j (*black lines*) plots shown in *E* were obtained at ϖ_{res} of 4000 (*circles*), 400 (*diamonds*), and 200 mV (*triangles*). The inset in *E* highlights g_{ss} increase with increase of V_j.

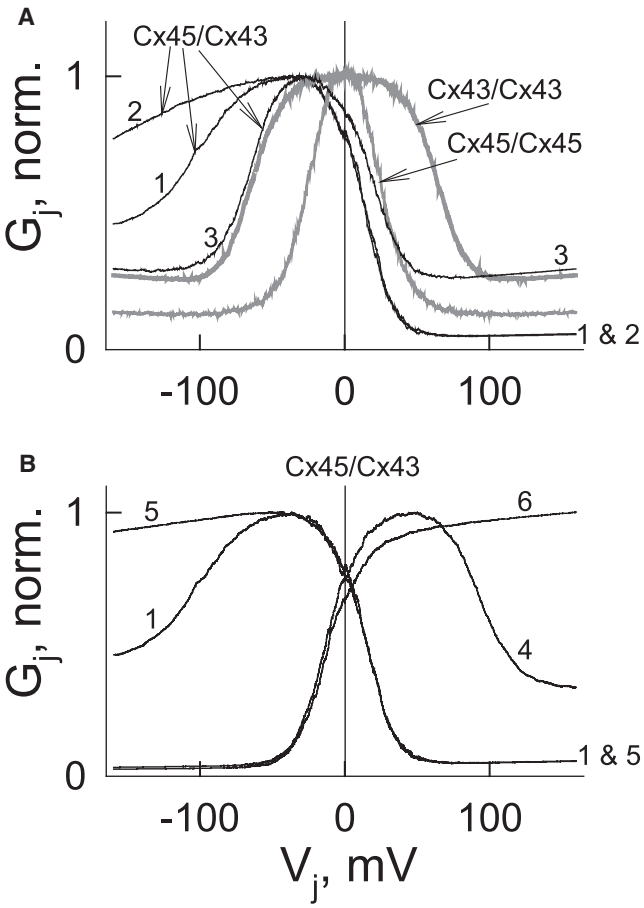

FIGURE 10 Simulation of V_j-gating in heterotypic junctions. (*A*) Shown demonstrates that V_j-gating asymmetry of heterotypic GJs (*black lines*) depends on the ratio of unitary conductances of composing hemichannels. Gray lines show G_{ss}-V_j plots of presumptive Cx43 and Cx45 homotypic junctions. Solid black lines, 1–3, show g_{ss}-V_j plots at different unitary conductances of composing hemichannels. (*B*) V_j-gating at different gating polarities of composing hemichannels. Plots 1 and 4 were obtained when both gates had the same gating polarity, negative and positive, respectively. Plots 5 and 6 were obtained when both gates had different gating polarities, Cx45 negative and Cx43 positive (*5*) and Cx45 positive and Cx43 negative (*6*).

g_{ss}-V_j plot, we changed $\gamma_{h,o}$ and $\gamma_{h,res}$ of Cx45 hemichannel making it twofold smaller than shown in Fig. 9 *A*, i.e., $\gamma_{h,o} =$ 30 pS and $\gamma_{h,res} = 2$ pS (see g_{ss}-V_j plot 2;) or equal to Cx43 hemichannel, i.e., $\gamma_{h,o} = 220$ pS and $\gamma_{h,res} = 25$ pS (see g_{ss}-V_j plot 3). Indeed, when conductances of both hemichannels were equal, then the g_{ss}-V_j dependence of heterotypic junctions best matches the original prediction. However, when $\gamma_{h,o}$ of Cx45 hemichannel becomes increasingly lower than that of the Cx43 hemichannel, then we can see the following tendency: the V_j-gating sensitivity of Cx45 hemichannel increases (the right shoulder of g_j-V_j plot is shifted to the left), whereas V_j-gating sensitivity of Cx43 hemichannel decreases (the left shoulder of g_j-V_j plot also is shifted to the left). This phenomenon was demonstrated earlier (12,20) and was explained by the fact that the difference in unitary conductances of composing hemichannels results to higher

fraction of V_j to drop across the hemichannel with smaller conductance, making this hemichannel virtually more sensitive to V_j. Our model fully supports the proposed mechanism. Therefore, unitary conductances of Cxs should be taken into account when efforts are made to find gating polarity of Cxs from gating profiles of homo- and heterotypic junctions.

All G_j-V_j plots shown in Fig. 10 *A* were simulated assuming that gating polarity of Cx43 and Cx45 hemichannels is negative as it has been shown experimentally (26). Fig. 10 *B* demonstrates how changes in gating polarity affect V_j-gating; all other parameters remained the same as shown in Fig. 9 *A*. Plots 1 and 4 in Fig. 10 *B* were obtained when both gates had negative and positive gating polarity, respectively. Plots 5 and 6 were obtained when both gates had different gating polarities, Cx45 negative and Cx43 positive (5), and Cx45 positive and Cx43 negative (6). Thus, the model can help to determine whether Cxs composing heterotypic junctions exhibit the same or different gating polarities.

Modulation of electrical signal cell-to-cell transfer asymmetry in heterotypic junctions

Fig. 11 *A* shows experimental recordings of voltage in HeLaCx45 (V_1) and HeLaCx40-CFP (V_2) forming heterotypic Cx40/Cx45 junctions. Repeated 80 mV voltage steps of positive and negative polarity were applied to cell-1 (V_1) patched in whole-cell voltage clamp configuration and electrotonic response was measured in cell-2 patched in the current-clamp configuration. It is evident that signal transfer can be modulated from virtually unidirectional to bidirectional by increasing the holding potential in the cell expressing Cx45; arrows show moments when the holding potential was increased stepwise. We have reported similar signaling asymmetry for Cx45/Cx31 (27) and Cx45/Cx43 (26) junctions and proposed that it is due to the V_j-gating asymmetry (12).

Fig. 11 *B* demonstrates simulation of signal transfer in heterotypic junction formed of Cxs with properties resembling Cx40 or Cx43 (cell-1) and Cx45 (cell-2). Both cells are in the voltage clamp mode. I_j trace shown in Fig. 11 *B* can be transformed into V_2 trace, similar to the one shown in Fig. 11 *A*, by multiplying I_j to the constant value of the input resistance of cell-2. The holding potential of cell-2 is always equal 0 mV. Three series of positive and negative pulses of 100 mV in amplitude were applied to cell-1. During the first series, when the holding potential of cell-1 is +15 mV, then I_j trace shows substantial signal transfer asymmetry determined as the ratio of I_js at the end of cycles with negative and positive V_j pulses, which was equal ~8.4. During the second and the third series of stimulation, when the holding potential of cell-1 was 0 mV and −15 mV, then signal transfer asymmetry decreased to 2.4 and 1.5, respectively. The bottom trace shows g_j change over time. At the beginnings of each series we assume that all channels are open, allowing the system to equilibrate before V_j steps are applied. This explains why each of three series starts with $g_j = 65$ nS. Thus, the model allows us to observe dynamics of g_j at $V_j = 0$ mV that is not possible to achieve in the experiment.

DISCUSSION

Our model is based on the V_j-gating concept initially proposed by Harris et al. (13) assuming that each hemichannel of GJ channel contain two oppositely oriented gates, which

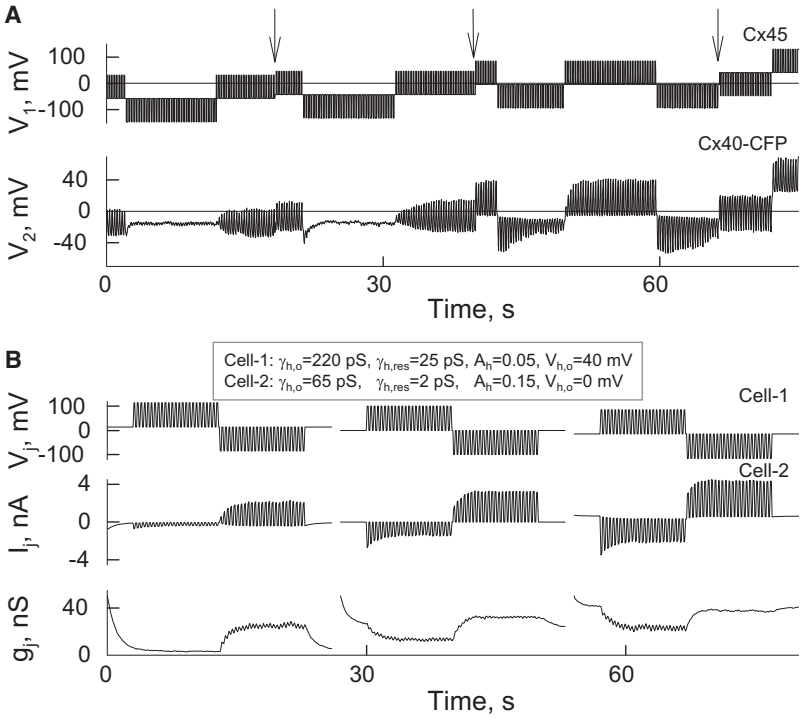

FIGURE 11 Experimental and simulated data demonstrating signal transfer asymmetry in heterotypic junctions. (*A*) Cell-to-cell transfer of electrical signal is modulated from unidirectional to bidirectional with changes in the holding potential of one of the cells. V_1 and V_2 are experimental traces of voltage recordings in Cx40-CFP/Cx45 junctions. Repeated voltage steps (~80 mV) of positive and negative polarity were applied to cell-1 (V_1), which is in whole-cell voltage clamp configuration. V_2 trace shows voltage recordings in cell-2, which is in current-clamp configuration. (*B*) Simulation of signaling asymmetry in heterotypic junctions. Both cells are in the voltage clamp mode. On top are shown parameters of cell-1 and cell-2 used in this simulation. Three series of positive and negative repeated pulses of 100 mV in amplitude were applied to cell-1. During the first series, when the holding potential of cell-1 is +15 mV, I_j trace shows signal transfer asymmetry equal ~8.4, which was determined as the ratio of I_js at the end of series with negative and positive V_j pulses. During the second and the third periods of simulation, when the holding potential of cell-1 was reduced to 0 mV and −15 mV, then signal transfer asymmetry decreased to 2.4 and 1.5, respectively. The holding potential of cell-2 was equal 0 mV.

operate based on contingent gating principles. Voltage gating properties of GJ channels were described using Boltzmann function proposing that GJ channels have two states, open and fully closed, as most of ionic channels. We used stochastic approach to calculate gating properties and assumed that the channel exhibits the residual conductance when V_j-gate is closed. Therefore, closing of the gate should not lead to the drop of entire V_j across a gated hemichannel. In 1993 it was shown, for the first time, that GJ channels in the insect cells during V_j-gating exhibit fast gating transitions between the open state and the substate called as a residual state (8,31). Soon after, V_j-gating to the substates was demonstrated also in mammalian cell lines expressing Cx43 (7), Cx40 (32), and even between cells expressing different Cxs and forming Cx26/Cx32 heterotypic GJs (33). Later, more members of Cx family were cloned and it was shown that γ_o can vary from ~10 to 300 pS (4). These new data made evident that during V_j gating of heterotypic junctions the single-channel conductance is an important factor, which can define V_j distribution inside the channel pore, i.e., hemichannel with smaller conductance will see across it higher proportion of V_j and experience more extensive gating, whereas voltage gating of hemichannels with larger conductance will be less affected by V_j.

In this model, like in one of Chen-Izu et al. (15), we take into consideration that only the fast gates that close channels to the substate are in operation. Simulation at the single-channel level revealed that nonrectifying homotypic GJ channel has one conductance for γ_o (both hemichannels open) and two conductances for γ_{res}, whereas rectifying channels are potential to exhibit unlimited number of unitary conductances of γ_o and γ_{res}. Furthermore, γ_{res} varied in much broader range than γ_o as it is shown in Fig. 6 *B*. Thus, these data may explain some discrepancies of single-channel conductance for open and residual states reported by different groups for the same type of Cx isoform. The simulation also revealed that the ratio, $\gamma_{h,res}/\gamma_{h,o}$, for the hemichannel is approximately twice smaller than a corresponding ratio, γ_{res}/γ_o, for GJ channel, which is ~1/4–1/5. This suggests that at the residual state the channel pore is closed at higher degree than could be predicted from the ratio, γ_{res}/γ_o. For example, if $\gamma_{h,res}/\gamma_{h,o} = 1/10$, then we can presume that only ~1/10 of cross-section of the hemichannel pore is open; assuming that the gate closes the hemichannel pore uniformly along its length. If the gate occupies only the small fraction of the pore then, to maintain the same ratio, narrowing of the pore during gating could be even bigger. This may create significant size-limited restrictions for macromolecules to permeate the channel gated to the residual state and explain no permeability of the residual state to dyes that permeate the open state (34,22). Otherwise, it could be assumed that permeability for dye molecules should be reduced proportionally with the ratio, γ_{res}/γ_o.

Data shown in Fig. 7 demonstrate the influence of each of independent parameters of the model on the V_j-gating properties of GJ channels. When $V_{h,o}$ changed from 80 to −30 mV that is equivalent to the shift of g_h-V_j curve along the V_j axis, this reduced g_{max} and the width of the bell shaped g_{ss}-V_j plot. The reduction of A_h from 0.2 to 0.01 mV^{-1} strongly affected the maximal steepness of g_{ss} decline ($\Delta g_{ss}/\Delta V_j$) and reduced g_{max}. The reduction of $\gamma_{h,res}$ from 40 to 5 pS affected mainly g_{min}. Simulation showed that $\gamma_{h,o}$ rectification minimally affected g_{in} in homotypic GJs. With V_j increase, $\gamma_{h,o,L}$ of left-side hemichannel increases and $\gamma_{h,o,R}$ of right-side hemichannels decreases (see Fig. 7 *D*) resulting to small or no change of g_{in} over V_j. Therefore, it is problematic detecting $\gamma_{h,o}$ rectification from g_{in}-V_j plots of homotypic junctions. Otherwise, in heterotypic junctions, hemichannel with lower conductance dominates in defining g_{in} and GJ channel can exhibit well expressed γ_o rectification if $\gamma_{h,o}$ rectifies (see Fig. 9 *D*). These conclusions are in full concert with earlier modeling studies (14). There are several reports demonstrating γ_o or g_{in} rectification of heterotypic GJ channels (35,33,36,37), and one example is shown in Fig. 3 *B*. $\gamma_{h,res}$ rectification had no evident effect on g_{in} but affected most significantly g_{ss} at higher V_js (see Fig. 7, *E–F*).

Though most of data shown in Fig. 7 could be intuitively predicted, some of them were unanticipated to us. For example, V_j-gating weakens or virtually disappears at $V_{h,o}$s below 30 mV (see Fig. 7 *A*) or at A_hs below ~0.02 (see Fig. 7 *B*). This may explain some of our unexpected observations when during partial recovery from uncoupling by CO_2, arachidonic acid or other uncouplers, we observed g_j recovery but with strongly reduced V_j-gating. Another informative conclusion comes from Fig. 7 *A*. At $V_{h,o}$s close to 0 mV, g_{max} is ~1/2 of that if all channels would be open. Thus, at $V_j = 0$ mV, only a fraction of channels are open. This phenomenon is also well illustrated in Fig. 10 *A* demonstrating V_j-gating of heterotypic junctions. g_j increased ~25% by changing V_j from 0 to ~−30 mV also suggesting that only a fraction of channels were open at $V_j = 0$ mV. Experiments with Cx45 homotypic GJs revealed that at $V_j = 0$ mV only ~50% of channels are closed due to the open channel probability being much below 1 (26). More recent data show that other Cxs, such as Cx45, Cx46, or Cx57, show similar properties (F. F. Bukauskas, unpublished data). For this reason, differently from earlier models of V_j-gating, we used a lag time allowing channels to equilibrate to the steady state (see g_j traces in Figs. 9 *B* and 11 *B*). We suppose that would be incorrect to apply V_j protocol without reaching a steady state at $V_j = 0$ mV, and even more for Cxs exhibiting high V_j-gating sensitivity, such as Cx37, Cx45, or Cx57.

For the simulation of a heterotypic junctions, we used two sets of parameters that are close to those of Cx43 (cell-1) and Cx45 (cell-2). Most of heterotypic junctions demonstrate a strong V_j-gating asymmetry illustrated in Figs. 4 and 9. In all examined heterotypic junctions that contain on one side Cx45, such as Cx31/Cx45, Cx40/Cx45, Cx43/Cx45 ((27); reviewed in (12)), or Cx36/Cx45 and Cx47/Cx45 (F. F. Bukauskas, unpublished data), we observed cell-to-cell electrical signal

transfer asymmetry that can be modulated from virtually unidirectional to bidirectional by changing the difference in holding potentials (ΔV_h) between coupled cells as illustrated in Fig. 11 *A*. Simulation data shown in Fig. 11 *B* confirm that V_j-gating asymmetry is one of the key factors defining such signaling asymmetry and that it can be effectively modulated by ΔV_h.

Previously, V_j-gating asymmetry of heterotypic junctions was commonly used to determine the gating polarity of Cxs assuming that V_j-gating of heterotypic junctions is a derivative of intrinsic gating properties of composing hemichannels. Our data show that this may be true only if the conductance of composing hemichannels is equal. When $\gamma_{h,o}$ of one hemichannel becomes increasingly lower than $\gamma_{h,o}$ of other hemichannel, then V_j-gating sensitivity of the first hemichannel increases whereas V_j-gating of the second hemichannel decreases (see Fig. 10 *A*). This phenomenon was demonstrated earlier (12,20) and was explained by the fact that the difference in unitary conductances of composing hemichannels results to higher fraction of V_j to drop across the hemichannel with smaller conductance, making this hemichannel virtually more sensitive to V_j. Thus, the contingent gating model in broad interpretation assumes that hemichannel with smaller conductance will see across it higher proportion of V_j and experience more extensive gating, whereas voltage gating of hemichannels with larger conductance will be less affected by V_j. Fitting of the experimental data to the model allows to estimate parameters defining V_j-gating sensitivity of composing hemichannels ($V_{h,o}$ and A_h) as well as their gating polarities from experimentally defined g_j-V_j dependence. It was proposed that the gating polarity of the fast gating mechanism is governed by charged residues in the N-terminal domain (30,38), and that this polarity could be reversed independent from the slow gating mechanism (23). Modifications of Cx43, including deletion of the carbocyl-terminus (CT) domain (39) or attachment of aequorin or an enhanced green fluorescent protein (EGFP) to CT, selectively abolishes fast gating to the residual state (40,17). Therefore, the location of the fast gate remains to be determined, and in this process, knowledge of the gating polarity of each Cx isoform is essential.

Presented data demonstrate that the model helps to find more details about the gating process and extrapolate gating properties of hemichannels composing GJ from experimentally defined g_{in}-V_j and g_{ss}-V_j plots. In addition, the model allows seeing dynamics of g_j during time periods when $V_j = 0$. This is highly supportive information in defining g_j dynamics before V_js protocol is applied or after g_j recovery to the steady state after V_j-gating. Experiments do not allow doing so without applying V_j. Significant improvement of this model relies on its ability to describe the kinetic behavior of channels, to simulate V_j-gating properties at the single-channel level or having unlimited number of channel in the junctions. The model also provides a practical formalism for fitting the voltage-gating profile over the entire voltage range, eliminating the previous need for data splicing for different V_j polarities. The proposed model also applies relatively easily to study V_j-gating of hemichannels simply by increasing $\gamma_{h,o}$ and $V_{h,o}$ of one of composing hemichannels to infinity. Furthermore, assuming that each hemichannel in this model corresponds to the half of unapposed hemichannel, and that one gates imitates the fast gate that closes to the residual state whereas the second gate imitates the slow gate that closes to the fully closed state ($\gamma_{h,res} = 0$), then the model can be used to simulate gating of unapposed hemichannels containing both fast and slow gating mechanisms. Thus, this model presents a useful tool for quantitative characterization of V_j-gating in GJ channels and unapposed hemichannels.

Limitations of the model and future directions

Although our model takes into consideration many of GJ channel properties, such as $\gamma_{h,o}$, $\gamma_{h,res}$, $V_{h,o}$, A_h, conductance rectification and gating polarity, still there is room for its improvement. This model applies to channels exhibiting one substate called as the residual conductance but not to channels exhibiting multiple substates. One of the ways to do so would be to introduce the gate that is composed of six subunits (each hemichannel is a hexamer of connexins) similar to that proposed earlier (41). It remains unclear whether there is a cooperative interaction between gating subunits and whether it depends on V_j.

The proposed model was adapted to cells that form one type of GJ channels. The model can be expanded to junctions that have in parallel several types of homotypic and/or heterotypic GJ channels. In parallel, introducing a slow gating mechanism in addition to the fast gate would be one of major steps for improvement. We are in the process of introducing such a model. When each hemichannel contain two gates instead of one, the calculation time is in the range of tens of minutes instead of seconds (this time also depends on number of channels and V_j protocol; see Fig. S1, Fig. S2, and Fig. S3 in Supplement 1). In addition, there are several problems that need to be solved. The location of the fast and slow gates, their interaction, and what fraction of V_j drops on each of them remains unclear. These questions can be at least partially solved by fitting a variety of experimental data with different versions of the model.

SUPPORTING MATERIAL

Three supplements, five figures, and two references are available at http://www.biophysj.org/biophysj/supplemental/S0006-3495(09)00666-3.

This work was supported by National Institutes of Health grants R01 NS036706 and RO1HL084464 (to F.F.B.).

REFERENCES

1. Lo, C. W. 2000. Role of gap junctions in cardiac conduction and development: insights from the connexin knockout mice. *Circ. Res.* 87:346–348.

2. Dermietzel, R., M. Kremer, G. Paputsoglu, A. Stang, I. M. Skerrett, et al. 2000. Molecular and functional diversity of neural connexins in the retina. *J. Neurosci.* 20:8331–8343.
3. Sohl, G., S. Maxeiner, and K. Willecke. 2005. Expression and functions of neuronal gap junctions. *Nat. Rev. Neurosci.* 6:191–200.
4. Kreuzberg, M. M., K. Willecke, and F. Bukauskas. 2006. Connexin-mediated cardiac impulse propagation: connexin 30.2 slows atrioventricular conduction in mouse heart. *Trends Cardiovasc. Med.* 16:266–272.
5. Spray, D. C., A. L. Harris, and M. V. Bennett. 1981. Gap junctional conductance is a simple and sensitive function of intracellular pH. *Science.* 211:712–715.
6. Bennett, M. V., and V. K. Verselis. 1992. Biophysics of gap junctions. *Semin. Cell Biol.* 3:29–47.
7. Moreno, A. P., M. B. Rook, G. I. Fishman, and D. C. Spray. 1994. Gap junction channels: distinct voltage-sensitive and -insensitive conductance states. *Biophys. J.* 67:113–119.
8. Weingart, R., and F. F. Bukauskas. 1993. Gap junction channels of insects exhibit a residual conductance. *Pflugers Arch.* 424:192–194.
9. Spray, D. C., A. L. Harris, and M. V. Bennett. 1981. Equilibrium properties of a voltage-dependent junctional conductance. *J. Gen. Physiol.* 77:77–93.
10. Bukauskas, F. F., and C. Peracchia. 1997. Two distinct gating mechanisms in gap junction channels: CO_2-sensitive and voltage-sensitive. *Biophys. J.* 72:2137–2142.
11. Banach, K., and R. Weingart. 2000. Voltage gating of Cx43 gap junction channels involves fast and slow current transitions. *Pflugers Arch.* 439:248–250.
12. Bukauskas, F. F., and V. K. Verselis. 2004. Gap junction channel gating. *Biochim. Biophys. Acta.* 1662:42–60.
13. Harris, A. L., D. C. Spray, and M. V. L. Bennett. 1981. Kinetic properties of a voltage-dependent junctional conductance. *J. Gen. Physiol.* 77:95–117.
14. Vogel, R., and R. Weingart. 1998. Mathematical model of vertebrate gap junctions derived from electrical measurements on homotypic and heterotypic channels. *J. Physiol.* 510:177–189.
15. Chen-Izu, Y., A. P. Moreno, and R. A. Spangler. 2001. Opposing gates model for voltage gating of gap junction channels. *Am. J. Physiol. Cell Physiol.* 281:C1604–C1613.
16. Ramanan, S. V., P. R. Brink, K. Varadaraj, E. Peterson, K. Schirrmacher, et al. 1999. A three-state model for connexin37 gating kinetics. *Biophys. J.* 76:2520–2529.
17. Bukauskas, F. F., K. Jordan, A. Bukauskiene, M. V. Bennett, P. D. Lampe, et al. 2000. Clustering of connexin 43-enhanced green fluorescent protein gap junction channels and functional coupling in living cells. *Proc. Natl. Acad. Sci. USA.* 97:2556–2561.
18. Kreuzberg, M. M., G. Sohl, J. Kim, V. K. Verselis, K. Willecke, et al. 2005. Functional properties of mouse connexin30.2 expressed in the conduction system of the heart. *Circ. Res.* 96:1169–1177.
19. Teubner, B., J. Degen, G. Sohl, M. Guldenagel, F. F. Bukauskas, et al. 2000. Functional expression of the murine connexin 36 gene coding for a neuron-specific gap junctional protein. *J. Membr. Biol.* 176:249–262.
20. Rackauskas, M., M. M. Kreuzberg, M. Pranevicius, K. Willecke, V. K. Verselis, et al. 2007. Gating properties of heterotypic gap junction channels formed of connexins 40, 43 and 45. *Biophys. J.* 92:1952–1965.
21. Trexler, E. B., F. F. Bukauskas, M. V. L. Bennett, T. A. Bargiello, and V. K. Verselis. 1999. Rapid and direct effects of pH on connexins revealed by the connexin46 hemichannel preparation. *J. Gen. Physiol.* 113:721–742.
22. Bukauskas, F. F., A. Bukauskiene, and V. K. Verselis. 2002. Conductance and permeability of the residual state of connexin43 gap junction channels. *J. Gen. Physiol.* 119:171–186.
23. Oh, S., C. K. Abrams, V. K. Verselis, and T. A. Bargiello. 2000. Stoichiometry of transjunctional voltage-gating polarity reversal by a negative charge substitution in the amino terminus of a connexin32 chimera. *J. Gen. Physiol.* 116:13–31.
24. Trexler, E. B., F. F. Bukauskas, J. Kronengold, T. A. Bargiello, and V. K. Verselis. 2000. The first extracellular loop domain is a major determinant of charge selectivity in connexin46 channels. *Biophys. J.* 79:3036–3051.
25. Valiunas, V., and R. Weingart. 2000. Electrical properties of gap junction hemichannels identified in transfected HeLa cells. *Pflugers Arch.* 440:366–379.
26. Bukauskas, F. F., A. Bukauskiene, V. K. Verselis, and M. V. L. Bennett. 2002. Coupling asymmetry of heterotypic connexin 45/connexin 43-EGFP gap junctions: properties of fast and slow gating mechanisms. *Proc. Natl. Acad. Sci. USA.* 99:7113–7118.
27. Abrams, C. K., M. M. Freidin, V. K. Verselis, T. A. Bargiello, D. P. Kelsell, et al. 2006. Properties of human connexin 31, which is implicated in hereditary dermatological disease and deafness. *Proc. Natl. Acad. Sci. USA.* 103:5213–5218.
28. Moreno, A. P., G. I. Fishman, E. C. Beyer, and D. C. Spray. 1995. Voltage dependent gating and single channel analysis of heterotypic gap junction channels formed of Cx45 and Cx43. *In* Intercellular Communication through Gap Junctions, Progress in Cell Research. Y. Kanno, K. Kataoka, Y. Shiba, and Y. Shibata, editors. Elsevier Science Publishers, B.V., Amsterdam, The Netherlands. 405–408.
29. Bruzzone, R., J. A. Haefliger, R. L. Gimlich, and D. L. Paul. 1993. Connexin40, a component of gap junctions in vascular endothelium, is restricted in its ability to interact with other connexins. *Mol. Biol. Cell.* 4:7–20.
30. Verselis, V. K., C. S. Ginter, and T. A. Bargiello. 1994. Opposite voltage gating polarities of two closely related connexins. *Nature.* 368:348–351.
31. Bukauskas, F. F., and R. Weingart. 1993. Multiple conductance states of newly formed single gap junction channels between insect cells. *Pflugers Arch.* 423:152–154.
32. Bukauskas, F. F., C. Elfgang, K. Willecke, and R. Weingart. 1995. Biophysical properties of gap junction channels formed by mouse connexin40 in induced pairs of transfected human HeLa cells. *Biophys. J.* 68:2289–2298.
33. Bukauskas, F. F., C. Elfgang, K. Willecke, and R. Weingart. 1995. Heterotypic gap junction channels (connexin26-connexin32) violate the paradigm of unitary conductance. *Pflugers Arch.* 429:870–872.
34. Qu, Y., and G. Dahl. 2002. Function of the voltage gate of gap junction channels: selective exclusion of molecules. *Proc. Natl. Acad. Sci. USA.* 99:697–702.
35. Rubin, J. B., V. K. Verselis, M. V. Bennett, and T. A. Bargiello. 1992. Molecular analysis of voltage dependence of heterotypic gap junctions formed by connexins 26 and 32. *Biophys. J.* 62:183–193.
36. Oh, S., J. B. Rubin, M. V. Bennett, V. K. Verselis, and T. A. Bargiello. 1999. Molecular determinants of electrical rectification of single channel conductance in gap junctions formed by connexins 26 and 32. *J. Gen. Physiol.* 114:339–364.
37. Hopperstad, M. G., M. Srinivas, and D. C. Spray. 2000. Properties of gap junction channels formed by Cx46 alone and in combination with Cx50. *Biophys. J.* 79:1954–1966.
38. Ri, Y., J. A. Ballesteros, C. K. Abrams, S. Oh, V. K. Verselis, et al. 1999. The role of a conserved proline residue in mediating conformational changes associated with voltage gating of Cx32 gap junctions. *Biophys. J.* 76:2887–2898.
39. Elenes, S., A. D. Martinez, M. Delmar, E. C. Beyer, and A. P. Moreno. 2001. Heterotypic docking of Cx43 and Cx45 connexons blocks fast voltage gating of Cx43. *Biophys. J.* 81:1406–1418.
40. Martin, P. E., C. H. George, C. Castro, J. M. Kendall, J. Capel, et al. 1998. Assembly of chimeric connexin-aequorin proteins into functional gap junction channels. Reporting intracellular and plasma membrane calcium environments. *J. Biol. Chem.* 273:1719–1726.
41. Vogel, R., V. Valiunas, and R. Weingart. 2006. Subconductance states of Cx30 gap junction channels: data from transfected HeLa cells versus data from a mathematical model. *Biophys. J.* 91:2337–2348.